An Experimental Performance Investigation of an Ultra-Wideband Directional Antenna in the Microwave Imaging of Breast Cancer Tumor

Ali R. Celik [1], Muhammed B. Kurt [1], and Selcuk Helhel [2]

[1] Department of Electrical and Electronics Engineering
Dicle University, Diyarbakir, 21280, Turkey
ali.celik@dicle.edu.tr, bkurt@dicle.edu.tr

[2] Department of Electrical and Electronics Engineering
Akdeniz University, Antalya, 07058, Turkey
selcukhelhel@akdeniz.edu.tr

Abstract ─ The purpose of this study is testing the performance and success of a compact-sized, ultra-wideband and directional printed circular monopole antenna proposed in a previous study for detection of the small breast cancer tumors. For this aim, simple but basic experimental studies of the radar-based ultra-wideband microwave measurement system are presented. In the measurements, different breast phantoms that have low dielectric constant materials representing the fat tissue and high dielectric constant object representing the tumor are formed and used. The object is located at different positions and the reflected signals are observed. The mono-static system which uses the same antenna to perform both the transmitting and receiving task of the signals is preferred in the study. According to the measured frequency domain signals, the reflected energy increases when the tumor is present. According to the amplitude and phase of the time domain signals, the presence, position and size of the tumor are inferenced. In order to provide more clear information about the tumor, a sample image is also created by implementing delay-and-sum algorithm. Furthermore, specific absorption rate of the breast is discussed. In summary, the performance of the antenna is valid for using in the radar-based ultra-wideband microwave imaging with respect to its features of the size, bandwidth, directivity, and beamwidth.

Index Terms ─ Breast cancer, microwave measurement, radar imaging, scattering parameters, ultra-wideband antenna.

I. INTRODUCTION

The World Health Organization reported about the cancer types in females that the most prevalent one is the breast cancer throughout the world [1]. Breast cancer stages are usually expressed as a number on a scale of 0 through IV, success rate in the treatment according to the stage decreases as the stages progress from 0 to IV.

Hence, diagnosis at the early stages (when the tumor size is not larger than 20 mm) is very crucial in the breast cancer treatment [2].

Breast cancer detection is primarily made by X-Ray Mammography, Magnetic Resonance Imaging (MRI), and Ultrasound techniques. Also, radar-based ultra-wideband (UWB) microwave imaging (MI) method has lately become applicable for this aim [3-8]. In the microwave frequencies (in the range of 0.3 and 300 GHz), the breast tissue can pass more signals than other tissues such as brain and muscle. In addition, the breast can be illuminated with microwave sources and multiple measurements can be made thanks to its position in the body. Due to these characteristics, one of the most suitable organs to test the success of microwaves in imaging is the breast [9].

The radar-based UWB MI method differs from X-ray Mammography method by using nonionizing radiation and illuminating power even less than a mobile phone. Therefore, it is much safer and even easier as there is no need for compression in the imaging [10]. This method has a comfortable system in contrast to MRI method having some negative features such as long process and uncomfortable measurement environment. Radar-based UWB MI method is also intended to overcome the main disadvantage of the Ultrasound method which needs experienced physicians to interpret the results in order to prevent obtaining false-negative/positive results [11].

When an electromagnetic wave passes from one medium to another, one part of the wave passes to the second medium and the rest is reflected back from the surface. In order to find the reflected wave, the reflection coefficient (Γ) is calculated. If the wave impinges normally, the Γ value is calculated using (1). To find the impedance (η) values, (2) is used:

$$\Gamma = \frac{\eta_2 - \eta_1}{\eta_2 + \eta_1}, \tag{1}$$

$$\eta = \sqrt{\frac{\mu}{\varepsilon - j\frac{\sigma}{\omega}}}, \qquad (2)$$

where **μ** is the magnetic permeability of the medium, **ε** is the electrical permittivity, **σ** is the conductivity, and **ω** is the angular frequency [12].

When the values of η are put into place in the related equation with Γ, it will be seen that higher ε or σ increases the reflection. Since the ε and σ values of the tumor have much greater values compared to the healthy breast in the microwave frequencies, the presence of the tumor leads to an increase in the amount of the reflections that allows detection of the tumor. So, the main principle of the radar-based UWB MI method is based on the significant difference in the electrical properties of the malignant tumors and normal breast tissue in the microwave frequencies [13].

In the measurement system, an UWB pulse which includes low to high frequencies is used. The lower band ensures adequate depth of penetration while the higher band ensures the enough resolution of the images. Hence, both the deeply buried and small-sized tumor can be detected based on the broad frequency bands [14,15].

In the system, the breast is illuminated by UWB pulses. The presence, position and size of any tumor can be seen on the images which are obtained by collecting and processing the reflected signals.

The used antenna is very critical to radiate and receive the pulses in the radar-based UWB MI systems. These systems require compact-sized, UWB, stable and directive antennas as their sensors [16]. A printed circular disc monopole antenna (PCDMA) having these properties was developed in [17] for early detection of the breast cancer. Although the features of the antenna were demonstrated to be suitable for using in the MI systems, the required test measurements were not being performed to investigate the success of the antenna.

In this paper, the main purpose is to investigate how the antenna of [17] would perform when used in the radar-based UWB MI system. For this aim, the frequency and time domain signals are examined. Also, an image is created to show the size and position of the tumor.

In the measurements, the proposed antenna is expected to work as previously stated and is intended to show better performance than some similar studies.

II. MATERIAL AND METHODS

In the radar-based UWB MI systems, generally three different methods can be used. These are: mono-static, bi-static, and multi-static radar methods [18,19]. In this study, the mono-static system which uses the same antenna to perform both the transmitting and receiving task of the signals is preferred. Hence, S_{11} scattering parameters which enable the determination of the reflections are measured.

In this study, experimental measurements are made

to observe the performance of the PCDMA in sensing the small tumors. In the measurements, two different breast phantoms are used to mimic the electrical properties of the healthy breast fat tissue. A 6 mm sized plastic object filled with sea water is used to mimic malignant tumor. One of the formed phantoms is planar and the other is hemi-spherical. In the measurement configurations, the planar phantom is scanned by the antenna manually. However, in order to measure the hemi-spherical phantom, the antenna must be turned around the phantom 360 degrees to save the S_{11} data from different positions by using the turn table device.

The properties of the antenna, the structures of the phantoms and the information about the measurements are given in sub-headings.

A. Characteristics of the developed antenna

In the study of [17], a compact-sized PCDMA including circular patch and L-shaped ground plane was designed and printed on a FR4 substrate. In the design process, a parasitic element was added to the patch side and a number of slots were etched on the ground plane in order to improve the bandwidth and directivity of the antenna as proposed in [20].

Simulated and measured S_{11} parameters showed good agreement between 3 and 10 GHz. But the return loss (RL) shifted above the -10 dB in a small number of frequencies. It was reported that these disagreements were due to the uncertainties in the dielectric material, fabrication constrains, effects of soldering of SMA connector, measurement loss and accuracy rate of full-wave simulation program not to be 100%. In order to overcome these drawbacks, in this study we have reconstructed the antenna and soldered the connector more carefully. The measurements have been taken in an anechoic chamber this time. As a result of these operations, it is observed that the RL curve is drawn below the -10 dB line over the entire frequency range of 3-10 GHz. The simulated and measured S_{11} results of reconstructed antenna are given in Fig. 1.
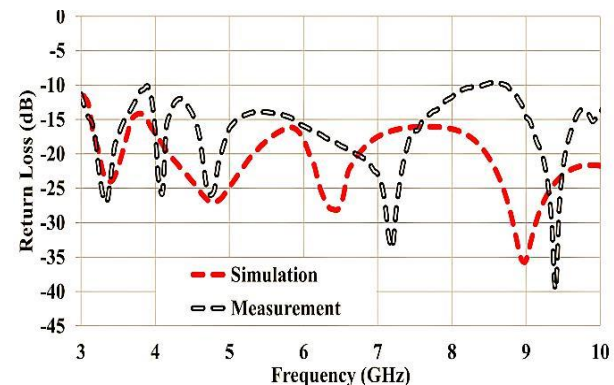

Fig. 1. The RL results of the antenna proposed previously in the study of [17] (after reconstruction).

When carefully examined, it is seen that the measured results shift systematically to higher frequencies according to the simulation. For this reason, a resonance that actually occurred before 3 GHz shifts to the 3-10 GHz frequency region. Therefore, a more resonance mode appears in the measurement results.

The RL results show that the proposed antenna is suitable for using in an MI system of the breast cancer with respect to the working frequency range. But, as mentioned before, the antenna does not only need to have broad bandwidth but also should have narrow half power beamwidth (HPBW) and stable directional radiation pattern to be used in a radar-based MI.

The directivity of the antenna changes between 6 dB and 9.4 dB in the 3-10 GHz; the radiation efficiency is higher than 90% over the entire band. Moreover, the antenna has both narrow HPBW and stable directional radiation pattern as seen in Fig. 2. These results show that the antenna is also suitable with respect to the radiation features for using in an MI system.

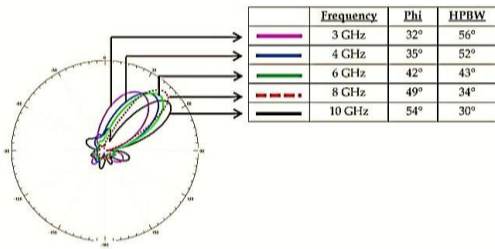| Frequency	Phi	HPBW
3 GHz	32°	56°
4 GHz	35°	52°
6 GHz	42°	43°
8 GHz	49°	34°
10 GHz	54°	30°

Fig. 2. Beam variation of the antenna proposed in [17].

In brief, the UWB directional antenna which was proposed in [17] is reconstructed and analyzed more carefully in this study. Here, we will present some experimental systems to investigate the capabilities of the antenna for the aim of using in the radar-based UWB MI of the breast cancer, which was not performed in [17].

B. Breast phantoms

As mentioned before, two different breast phantoms are formed and used in the experiments. One of these phantoms has rectangular shape, and the other has hemi-spherical. The dimension of the rectangular phantom is $15x5x7$ cm^3, and the radius of the hemi-spherical phantom is 6 cm.

Since the working frequency range is 3-10 GHz in this study, the electrical properties of the fat and tumor structures are based on according to approximately mean value of the range, 7 GHz. At this frequency, the relative permittivities (ε_r) of the fatty breast tissue and tumor are 4.2 and 64, respectively. Also, the σ of the breast tissue and tumor are 0.5 and 10 S/m, respectively [21,22]. Since the study is intended to determine the presence of the tumor, it is not necessary to add skin to the phantoms. A borosilicate glass with 2 mm thickness is used as skin

tissue in the planar phantom, whereas the hemi-spherical phantom contains only the tumor and fatty tissue.

There are some materials that possess close dielectric properties to the breast such as vegetable oils, pure glycerine, dry cornflour, beeswax, etc. Similarly, there are some materials having close dielectric properties to the tumor tissue such as agar, gelatine, sea-water, etc. In the rectangular phantom, we use canola oil having ε_r of 4 and σ of 0.3 S/m at 7 GHz [23,24] as a fat-mimicking material. However, in the hemi-spherical phantom, the beeswax having ε_r of 3 and σ of 0.1 S/m at 7 GHz [25-27] is preferred. The tumor-mimicking object is in the form of a plastic cylinder filled with sea-water having ε_r of 69 and σ of 9 S/m at 7 GHz [27] and is placed inside the phantoms similar to the studies of [27-29]. Since the dielectric properties of the plastic are similar to the properties of the oil, using the plastic material to keep sea-water does not affect the measurement results considerably [30].

C. Configurations of the measurements systems

This section explains the measurements on the phantoms by using the PCDMA. Throughout the measurements of the rectangular phantom, the antenna is placed 20 mm above the phantom. Throughout the measurements of the hemi-spherical phantom, the PCDMA is positioned at a height of 30 mm on the z-axis while the center coordinate of the sphere and tumor are (x=0, y=0, z=0 mm) and (x=0, y=0, z=30 mm), respectively. The distance between the phantom and the upper right corner of the antenna is set to 20 mm. The measurement systems are shown in Fig. 3 and Fig. 4.
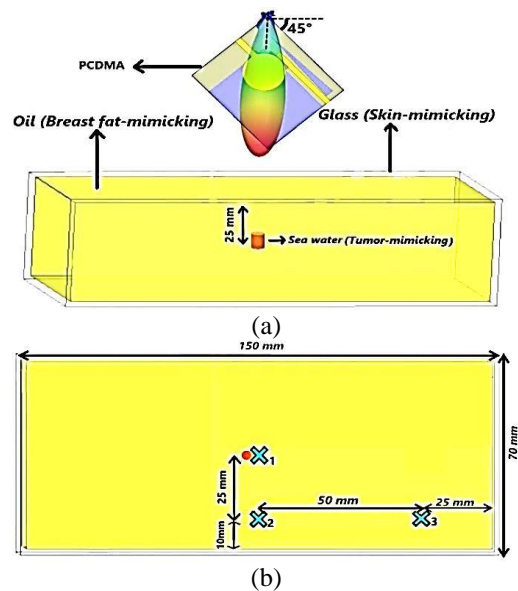

Fig. 3. Measurement configuration of the planar phantom: (a) front view with tumor, and (b) top view with tumor and measurement points.
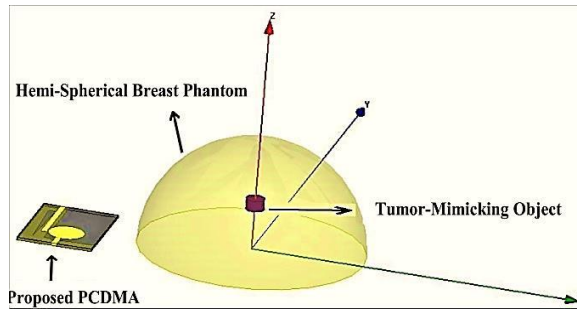
Fig. 4. Measurement configuration of the hemi-spherical phantom.

Firstly, the measurements are made when there wasn't a tumor in the phantoms. Then, the tumor-mimicking object is placed in the phantoms and the measurements are repeated as seen from Figs. 3 and 4. Since the direction of the main beam moves from $\varphi=32$ to $\varphi=54$ degrees as given from the Fig. 2, the antenna is positioned so that the direction of the main beam is as perpendicular as possible to the phantoms. In the measurements of the rectangular phantom, the measurement values recorded for different locations (X_1, X_2, X_3) as shown in Fig. 3 (b). In the measurements of the hemi-spherical phantom, the antenna is turned around the phantom 360 degrees by using the turn table, and the results are recorded one every 45 degrees.

III. MEASUREMENTS, RESULTS AND DISCUSSIONS

A. Experimental measurements

In the experiments, Anritsu MS2028C 10 kHz-20 GHz Vector Network Analyzer (VNA) and test port extension cable are used to send the microwave signals to the breast phantoms and to measure the signals reflected from them. Prior to the measurements, the VNA is calibrated over UWB (3-10 GHz in the present case) using a one-port calibration procedure [31]. The measurement systems using the rectangular and hemi-spherical phantoms are shown in Fig. 5 and Fig. 6, respectively.

The measurement of the planar phantom has been made in the laboratory. In order to minimize the reflections from the walls, desks and other equipments, two square absorbers (60x60 cm^2) and an isolation material is used during the measurement.

In the measurement of the hemi-spherical phantom, scanning the phantom 360 degrees is necessary to obtain successful results. For this aim, a turn table with an isolation material (foamed sealant) which is put to reduce the coupling effect and to align the phantom with the antenna is used in a fully anechoic chamber.
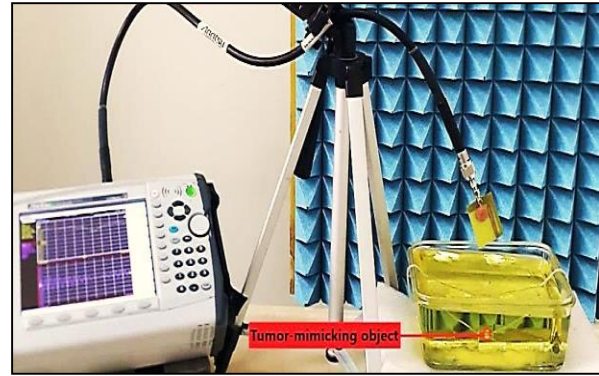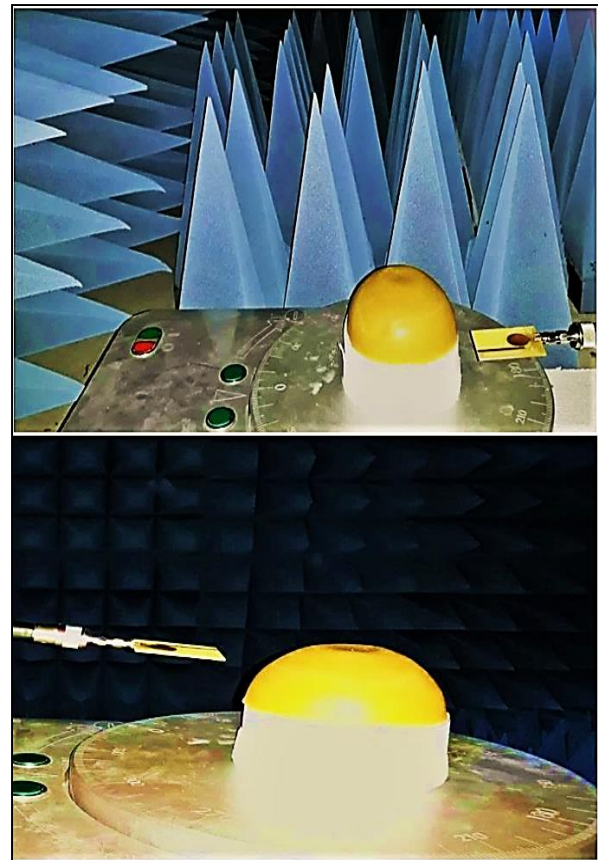

Fig. 5. The measurements for the planar phantom.

Fig. 6. The measurements for hemi-spherical phantom.

B. Results in the frequency domain

The measurement results for the planar phantom are given in the frequency domain. The measured S_{11} vs. frequency values for the cases of with and without tumor for the point of X_1 are shown in Fig. 7.

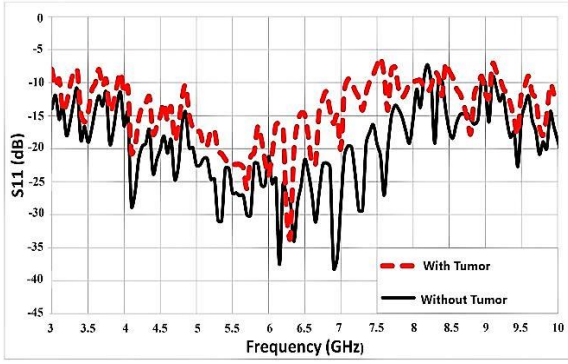Also, the recorded S_{11} values for three locations (X_1, X_2, and X_3) are plotted in Fig. 8.

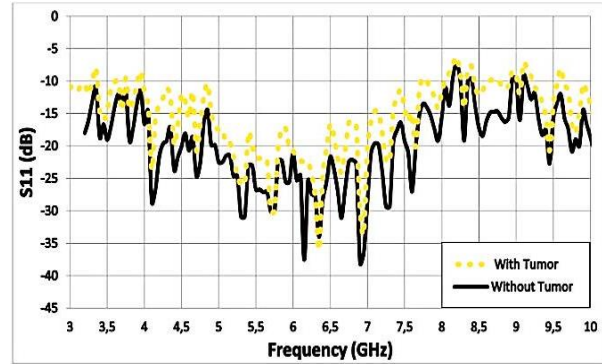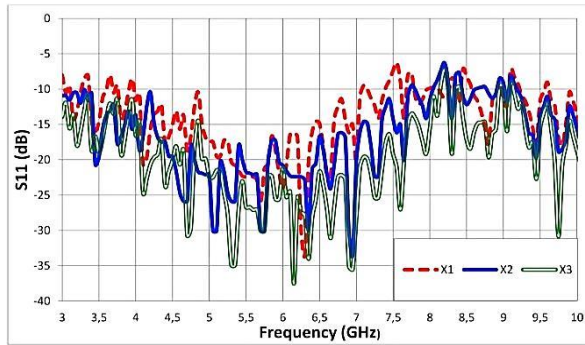Fig. 7. S_{11} results in the frequency domain (at X_1 point).

Fig. 8. S_{11} results for different locations (with tumor).

S_{11} and Γ values are related to each other according to the Equation (3) which means that the smaller the magnitude of S_{11}, the larger the reflection becomes [32]:

$$S_{11}(dB) = 20\log_{10}|\Gamma|. \qquad (3)$$

As given before, there are significant differences in the electrical properties of the tumor and normal breast tissue in the microwave frequencies. So, the transmission of the microwaves is less (means that the reflection is high) when the tumor is present. Hence, the magnitude of S_{11} decreases over the working frequency in the tumorous case as it is seen from the Fig. 7. Furthermore, it is understood from the Fig. 8 that the reflected energy decreases when the antenna moves away from the tumor and vice versa.

The RL differences between the tumorous and non-tumorous cases can be seen more clearly in the range of 6 to 8 GHz. Hence, another important deduction from the Figs. 7 and 8 is that the best frequencies for tumor detection are these frequencies. However, in the detection process, not only 6-8 GHz range is used, but also all frequencies of 3-10 GHz range are used.

In another experiment, the object which was previously placed at a depth of 25 mm is placed at a depth of 45 mm. Then the measurements are performed again. S_{11} results for the point of X_1 when the tumor is buried at a deeper position are shown in Fig. 9.

Fig. 9. S_{11} results for deeply buried tumor (at X_1 point).

C. Results in the time domain

The results for the hemi-spherical phantom are given in the time domain. In these measurements, a Gaussian pulse is emitted from the antenna. The pulse signal becomes narrower as the bandwidth of the antenna increases. Since the used antenna has the bandwidth of 7 GHz, it can send a narrow pulse signals. Thus, one of the processes required to obtain high resolution images is provided.

As mentioned before, the values of the reflected signals for tumorous and non-tumorous states are recorded in 8 positions where the antenna and tumor-mimicking object are at the height of 30 mm on the z axis. Since the object is at (x=0, y=0), the distance between the antenna and object remains same while the phantom is being scanned. So, the reflections from the 8 positions will be similar and showing one of the signals would be sufficient for observing the cases.

The emitted Gaussian signal and the reflected signal received by the antenna are shown in Fig. 10. Since a delay time would occur during the return of the transmitted signal, and the amplitude decreases due to the losses, it is seen from the Figs. 10 (a) and (b) that there are differences in the phase and amplitude of the sent and reflected signals. In the Fig. 10 (b), for the 1.5 to 2 ns interval, it is seen that the signal amplitude is higher in the tumorous case than amplitude of the non-tumorous case.
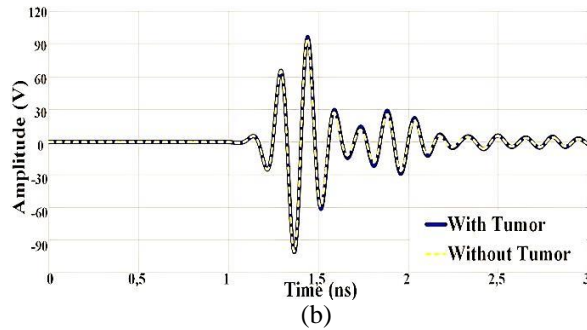

(a)
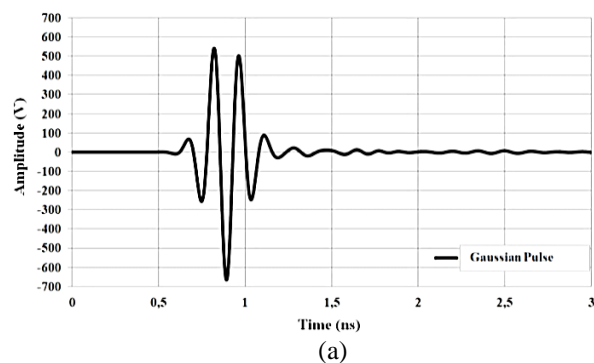
Fig. 10. (a) Gaussian pulse emitted from the antenna, and (b) reflected signals from the hemi-spherical phantom.

In another measurement, the tumor-mimicking object is placed at the point of (x=0, y=40, z=30) mm. Therefore, the distance between the antenna and object changes when the phantom is scanned. Hence, the signal values taken from 8 different points are at the different levels. The values when the antenna is at the closest and farthest to the tumor are given in Fig. 11.
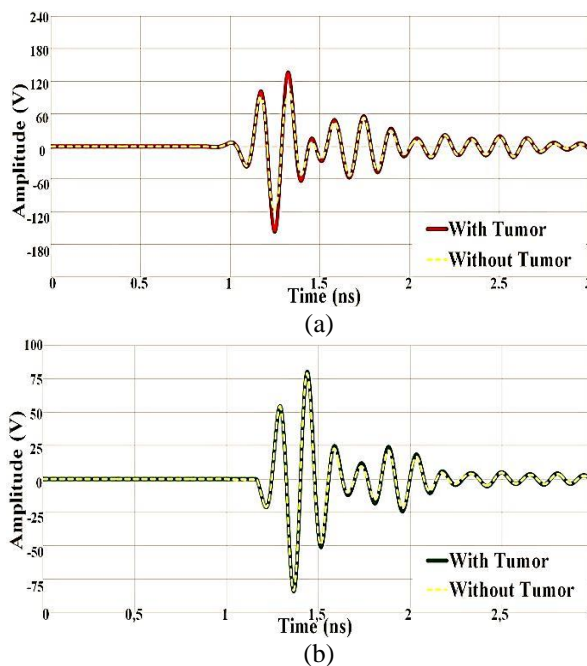

Fig. 11. Reflected time domain signals: (a) antenna is at the closest, and (b) antenna is at the farthest to the tumor.

As expected, it is seen from the Fig. 11 (a) that the amplitude of the reflected signal is higher in the tumorous case than amplitude obtained in the non-tumorous case. Further, since the tumor is closer to the surface and provides more reflections, this time the difference is greater than that of obtained in the Fig. 10 (b). Also, it is seen again that there is a phase difference between the Gaussian pulse and the reflected signal.

However, this time it is not as much as in Fig. 10 (b) since the signal reaches to the tumor and reflects back from it in a less time.

When Fig. 11 (b) is examined, it is seen that the amplitude of the reflected signal is higher in the tumorous case. But, since the tumor is at a point far away from the surface and provides less reflections, this time the difference is less than that of obtained in the Fig. 10 (b). Also, it is seen again that there is a phase difference between the Gaussian pulse and the reflected signal. Since the signal reaches to the tumor and reflects back from it in a longer time, this time it is more than that of seen in Fig. 10 (b).

For a better understanding of the graphs, the amplitude differences of the tumorous and non-tumorous cases between 1.5 and 2 seconds for the different positions of the tumor are given in Table 1. The maximum amplitudes and phase differences of the reflected signals are also given in Table 2.

Table 1: Amplitude differences between the reflected signals of tumorous and non-tumorous situations (V)

Time (ns) Tumor Position	1,6	1,75	1,9
Tumor is closest to the antenna	60–54=**6**	70–58=**12**	35–30=**5**
Tumor is at the center	30–27=**3**	19–15=**4**	31–27=**4**
Tumor is farthest to the antenna	29–27=**2**	18–16=**2**	30–28=**2**

Table 2: The maximum amplitudes and phase differences of the reflected signals

	Maximum Amplitude	Starting Time
Tumor is closest	130 V	0.9 ns
Tumor is at the center	95 V	1.1 ns
Tumor is farthest	80 V	1.25 ns

D. Imaging result

The measurements made up to this stage have been performed in the frequency and time domains. However, in order to make a more successful diagnosis, the obtained data must be converted into images.

The signals must be subjected to various processes such as pre-processing, filtering, calibration, energy calculation to create image. For this purpose, the calibration phase is carried out by taking the difference between the signal reflected from the tumor tissue and the signal reflected from the healthy tissue as suggested in the study of [33]. After obtaining the tumor response by the calibration process, the stage of obtaining the energy profile of the breast is started. For this aim, the

points in the breast are considered as pixels and the individual energies of these pixels are calculated. Then time delays are calculated and collected in order to determine the positions of the pixels. Finally, the image is created. In order to calculate the energy values, the delay-and-sum algorithm which has been used in many other studies like [34-36] is preferred.

As shown before, the time domain data from different positions have been obtained for the hemispherical phantom which has tumor-mimicking object at the (0, 0, 30 mm) position. The image that is created by using these data is given in Fig. 12. In the image, the object is seen as the black colour. It is known that the cylindrical object has a diameter of 6 mm and a height of 4 mm. So, it is expected to be seen as the size of 6 mm in the x-axis direction and the size of 4 mm in the z-axis direction. It is displayed as 6.6 mm and 3.6 mm in the created image. Hence, the size is determined with an accuracy rate of 90%. The center position of the object is displayed at the points of (x=-1 and z=31 mm) which is actually at the points of (x=0 and z=30 mm). Therefore, it can be said that the position is also determined with very high accuracy.
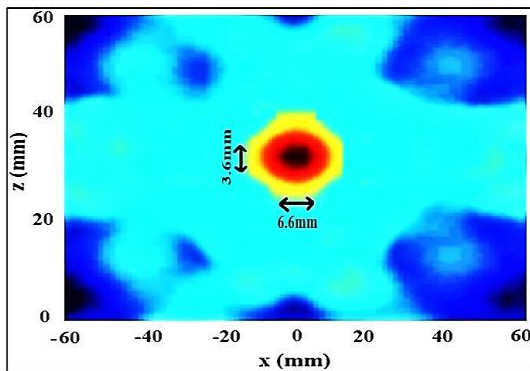

Fig. 12. A sample image showing the size and position of the tumor placed at the point of (x=0, y=0, z=30) mm.

E. Specific absorption rate considerations

Specific Absorption Rate (SAR) means a measure of the rate at which energy is absorbed by the human body when exposed to the electromagnetic field [37,38]. It is defined as the power absorbed per mass of tissue as expressed in (4):

$$SAR = \frac{\sigma|E|^2}{\rho}, \qquad (4)$$

where σ is the conductivity (S/m) of the tissue, E is the internal electric field (V/m), and ρ is the mass density (kg/m^3).

It is necessary to observe whether the power levels for the operation of microwave breast cancer detection systems are lower than the acceptable SAR levels. International Commission on Non-Ionizing Radiation Protection (ICNIRP) accepts the SAR value to be 0.4 w/kg for those who are exposed to electromagnetic fields as a matter of professions (in controlled environment), and 0.08 w/kg for the public population (in uncontrolled environment). In addition to the limit values of whole body (WB), the limits of local SAR over 1g and 10g of the tissues are also determined [39]. These values are displayed in Table 3.

Table 3: SAR exposure limits in different environments

	SAR$_{WB}$	SAR$_{1G}$	SAR$_{10G}$
Controlled Environment	0.4	8	20
Uncontrolled Environment	0.08	1.6	4

Since the aim of this study is to make a measurement for breast tumor detection which is intended to be used in the hospitals, the standards for the controlled environment should be considered. Also, the tumor detection measurements involve the exposure of the breast to the electromagnetic fields locally. So, it is crucial to ensure that peak SAR values conform to the standards set for the maximal peak averaged over a small amount of mass as opposed to WB average [40].

In this study, the SAR distributions are obtained for 1.0g volume of tissue with the aid of HFSS program. According to the simulation results obtained at 7 GHz, the maximum average SAR1g value of fatty tissue without tumor is 1.2292 W/kg. When the 6 mm sized tumor is located to the (0,0,30 mm) point, the maximum average SAR1g values of the fatty tissue and tumor are 3.6091 W/kg and 6.8817 W/kg, respectively. The results show that, the SAR values of the breast tissue for the tumorous and non-tumorous cases are below the determined limit values.

It is seen from the SAR values that a large amount of power is absorbed on the tumor concealed area due to the high dielectric property of the tumor tissue. Similarly, the SAR values over the breast fat are lower for non-tumorous case compared to the tumorous case. So, it is understood that measuring the SAR values is helpful to determine the presence and position of the tumor. The maximum SAR coordinate in the breast with 6 mm tumor is obtained as (-1.8, 2.1, 28.8 mm) where the actual center position of tumor is (0, 0, 30 mm). Hence, the coordinates of the corresponding maximum value of SAR can be identified for detecting the locations of tumor inside the breast.

F. Comparison with the similar studies

Several compact-sized UWB antenna designs have been proposed for the radar systems, see-through-wall imaging, wireless communications applications, cognitive radio applications, C and X bands operations, and medical imaging [41-60]. Each has its own advantages

and drawbacks. Some of these antennas exhibit omnidirectional radiations whereas some others have directional radiation patterns. For the performance analysis of the used PCDMA, a comparison with the antennas of [41-60] is given in Table 4. According to this table, the bandwidth is increased, the HPBW values are reduced and the directivity is improved with compared to the some works reported in the literature.

In the studies of [53-60], not only antenna designs were made, but also measurements were performed for the breast cancer detection. Thus, the performances of

the antennas in the MI systems were investigated. But, many conditions such as measurement environments, designed antennas, constructed phantoms, used VNA devices and the methods preferred for the image generation are different in these studies. Hence, it is not possible to compare the results of our study clearly with the results given in other studies. However, we have tried to make a comparison with the studies [53-60] that have the systems which are similar to our study with respect to the measurement environment and phantom structures. These comparisons are given in Table 5.

Table 4: Comparison of the performance of the used antenna with the antennas reported in some previous work

Reference Antenna	Size (mm)	Frequency Band (GHz)	Bandwidth (%)	Radiation Type	HPBW Moves (°)	Gain (dB)
[41]	32 x 30	3.1 - 14.0	127.5	Omnidirectional	--- [1]	2.2 - 6.0
[42]	32 x 24	3.9 - 11.0	114	Omnidirectional	--- [1]	1.7 - 5.3
[43]	32 x 24	2.7 - 12.0	126.5	Omnidirectional	--- [1]	0.5 - 5.5
[44]	18 x 12	3.02 - 15.21	133	Omnidirectional	--- [1]	--- [1]
[45]	50 x 46	3.1 - 12.6	120	Directional	75 - 25	4.0 - 8.0
[46]	50 x 50	6.0 - 8.0	28	Directional	47 - 37	--- [1]
[47]	32 x 30	4.2 - 8.5	68	Directional	78 - 43	5.2 - 9.3
[48]	50 x 50	4.0 - 9.0	77	Directional	56 - 25	7.0 - 10.0
[49]	40 x 26	1.0 - 8.0	155	Directional	--- [1]	--- [1]
[50]	50 x 50	4.1 - 11.5	95	Directional	49 - 22	2.5 - 8.4
[51]	50 x 50	3.1 - 11.0	112	Directional	--- [1]	4.3 - 10.8
[52]	50 x 40	3.0 - 8.0	91	Directional	60 - 40	5.0 - 6.8
[53]	62.5 x 62.5	2.0 - 4.0	66	Directional	--- [1]	--- [1]
[54]	50 x 50	2.75 - 11.0	126	Directional	--- [1]	--- [1]
[55]	36 x 36	2.5 - 10.4	122	Directional	--- [1]	1.0 - 9.0
[56]	40 x 40	3.6 - 8.0	76	Directional	--- [1]	3.8 - 7.0
[57]	73.5 x 42	3.0 - 10.0	108	Directional	--- [1]	2.5 - 10.0
[58]	27.3 x 14	4.5 - 10.5	80	Directional	--- [1]	--- [1]
[59]	63 x 51	2.5 - 8.5	109	Directional	--- [1]	2.0 - 7.5
[60]	80 x 44	2.4 - 18.0	153	Directional	--- [1]	--- [1]
Used Antenna	**55 x 40**	**3.0 - 10.0**	**108**	Directional	**56 - 30**	**6.0 - 8.4**

Table 5: Comparison of the performance of this study with the measurements reported in some previous work

Reference	Antenna Type	Phantom Type	Shape and Size of the Tumor
[53]	Bow-tie	With Skin (2 mm)	Ellipsoid - (L=15mm & W=5mm)
[54]	Probe	With Skin (Thin)	Spherical - 5 mm
[55]	Tapered-Slot	Without Skin	Cylindrical Pipe (H=20mm & R=5mm)
[56]	Planar Plate	With Skin (4 mm)	Cylindrical - 4.5 mm
[57]	Slotted Vivaldi	With Skin (1 mm)	Spherical - 10 mm
[58]	Vivaldi	With Skin (2 mm)	Spherical - 10 mm
[59]	Vivaldi	With Skin (Thin)	Cylindrical Pipe (H = 20mm & R = 2.5mm)
[60]	Antipodal Vivaldi	With Skin (Thin)	Cylindrical - 16 mm
This Study	**PCDMA**	**With Skin in Planar & Without Skin in Hemi-Spherical**	**Cylindrical - 6 mm**

IV. CONCLUSION

In this study, firstly it was mentioned that the success rate of the breast cancer treatment is very high if it is detected at an early stage. Then, early detection methods of the breast cancer were introduced. The radar-based UWB MI system which is one of the emerging methods was explained in detail. After that, it was emphasized that the used antenna is very critical to radiate and receive the pulses in this system.

In the study, the compact-sized UWB directional antenna was used in the experimental measurements and the performance of it was investigated which was the main purpose of this study. For the experiments, the breast phantoms with different shapes and materials were formed. A 6 mm object having similar electrical properties to the malignant tumor was placed in the phantoms, and the measurements have been made in the different domains. According to the both frequency and time domain results, it was concluded that the presence of the tumor could be clearly determined. In addition, inferences about the position and size could be made. But, in order to make more clear observation, the reflected signals were converted into image. Thus, the location and size of the tumor was detected successfully. Hence, the other aim of the study was achieved. Furthermore, SAR consideration for the breast was made. As a conclusion, in this study it was demonstrated that the UWB and directive PCDMA is capable of detecting small tumors in a radar-based UWB microwave breast cancer detection system which is a new method having some features supporting existing detection methods.

ACKNOWLEDGMENT

REFERENCES

[1] World Health Organization: WHO, Breast cancer awareness, Available: http:// www.who.int/cancer/ breast_cancer_awareness/en, 2017.

[2] M. Weiss, "Your guide to the breast cancer pathology report," http://www.breastcancer.org, 2017.

[3] E. C. Fear and M. A. Stuchly, "Microwave detection of breast cancer," *IEEE Transactions on Microwave Theory and Techniques*, vol. 48, pp. 1854-1863, 2000.

[4] X. Li and S. C. Hagness, "A confocal microwave imaging algorithm for breast," *IEEE Microwave and Wireless Components Letters*, vol. 11, pp. 130-132, 2001.

[5] E. J. Bond, X. Li, S. C. Hagness, and B. D. Van Veen, "Microwave imaging via space-time beamforming for early detection of breast cancer," *IEEE Transactions on Antennas and Prop.*, vol. 51, pp. 1690-1705, 2002.

[6] M. Klemm, I. Craddock, J. Leendertz, A. Preece, and R. Benjamin, "Radar-based breast cancer detection using a hemispherical antenna array-experimental results," *IEEE Transactions on Antennas and Propagation*, vol. 57, pp. 1692-1704, 2009.

[7] A. K. Alqallaf, R. K. Dib, and S. F. Mahmoud, "Microwave imaging using synthetic radar scheme processing for the detection of breast tumors," *Applied Computational Electromagnetics Society (ACES) Journal*, vol. 31, no. 2, pp. 98-105, 2016.

[8] S. Sadeghi and R. Faraji-Dana, "A practical UWB microwave imaging system using time-domain DORT for tumor detection," *ACES Journal*, vol. 31, no. 6, pp. 692-699, 2016.

[9] O. Güren, "Surface impedance based microwave imaging method for breast cancer screening," *Istanbul Technical University*, Turkey, *PhD*, 2014.

[10] E. C. Fear, X. Li, S. C. Hagness, and M. A. Stuchly, "Confocal microwave imaging for breast cancer detection: Localization of tumors in three dimensions," *IEEE Transactions on Biomedical Engineering*, vol. 49, pp. 812-822, 2002.

[11] A. R. Celik, "Detection of the breast tumors by ultra-wideband radar based microwave method," *Dicle University*, Diyarbakir, Turkey, *PhD*, 2018.

[12] F. Ulaby, *Fundamentals of Applied Electromagnetics*. Prentice Hall, Washington DC, 2006.

[13] M. Islam, M. T. Islam, M. R. I. Faruque, M. Samsuzzaman, N. Misran, and H. Arshad, "Microwave imaging sensor using compact metamaterial UWB antenna with a high correlation factor," *Materials*, vol. 8, pp. 4631-4651, 2015.

[14] X. Xiao and T. Kikkawa, "Influence of the organism interface on the breast cancer detection by UWB," *Applied Surface Science*, vol. 255, pp. 597-599, 2008.

[15] H. Zhang, T. Arslan, and B. Flynn, "A single antenna based microwave system for breast cancer detection: experimental results," *Loughborough Antennas & Propagation Conference*, UK, 2013.

[16] J. J. Golezani, "Directional wide band printed monopole antenna for use in microwave breast cancer imaging," *Istanbul Technical University*, *MS*, 2012.

[17] A. R. Celik and M. B. Kurt, "Development of a novel ultra-wideband, stable and high directive monopole disc antenna for radar-based microwave imaging of breast cancer," *Journal of Microwave Power and Electromagnetic Energy*, vol. 52, no. 2, pp. 75-93, 2018.

[18] J. M. Sill and E. C. Fear, "Tissue sensing adaptive

radar for breast cancer detection - experimental investigation of simple tumor models," *IEEE Trans. on Microwave Theory and Techniques*, vol. 53, pp. 3312-3319, 2005.

[19] Y. Xie, B. Guo, L. Xu, J. Li, and P. Stoica, "Multi-static adaptive microwave imaging for early breast cancer detection," *39th Asilomar Conference on Signals, Systems, and Computers*, CA, USA, 2005.

[20] Y. Li, W. Li, Q. Ye, and R. Mittra, "A survey of planar ultra-wideband antenna designs and their applications," in *Forum for Electromagnetic Research Methods and application Technologies (FERMAT)*, ID: Li-ART-2014-01-002, pp. 1-6, 2014.

[21] P. M. Meaney, K. D. Paulsen, A. Hartov, and R. K. Crane, "An active microwave imaging system for reconstruction of 2-D electrical property distributions," *IEEE Transactions on Biomedical Engineering*, vol. 42, pp. 1017-1026, 1995.

[22] I. Craddock, R. Nilavalan, J. Leendertz, A. Preece, and R. Benjamin, "Experimental investigation of real aperture synthetically organised radar for breast cancer detection," *IEEE on Antennas and Propagation Society International Symposium*, Washington, DC, USA, 2005.

[23] S. Adnan, R. A. Abd-Alhameed, M. Usman, C. H. See, J. M. Noras, and M. B. Child, "Simulation and experimental measurements for near field imaging," *Progress In Electromagnetics Research Symposium*, Malaysia, 2012.

[24] J. D. Garrett and E. C. Fear, "Average dielectric property anlaysis of complex breast tissue with microwave transmission measurements," *Sensors*, vol. 15, pp. 1199-1216, 2015.

[25] S. Vedantham, A. Karellas, G. R. Vijayaraghavan, and D. B. Kopans, "Digital breast tomosynthesis: State of the art," *Radiology*, vol. 277, no. 3, pp. 663-684, 2015.

[26] N. Kiarashi, A. C. Nolte, G. M. Sturgeon, W. P. Segars, S. V. Ghate, L. W. Nolte, E. Samei, and J. Y. Lo, "Development of realistic physical breast phantoms matched to virtual breast phantoms based on human subject data," *Medical Physics*, vol. 42, no. 7, pp. 4116-4126, 2016.

[27] B. J. Mohammed, "Design and implementation of microwave imaging systems for medical applications," *The University of Queensland School of Information Technology and Electrical Engineering*, Australia, *PhD*, 2014.

[28] M. E. Bialkowski, "Ultra wideband microwave system with novel image reconstruction strategies for breast cancer detection," *40th European Microwave Conference*, France, 2010.

[29] W. C. Khor and M. E. Bialkowski, "Investigations into cylindrical and planar configurations of a microwave imaging system for breast cancer

detection," *IEEE Antennas and Propagation Society International Symposium*, Albuquerque, 2006.

[30] B. Riddle, J. B. Jarvis, and J. Krupka, "Complex permittivity measurements of common plastics over variable temperatures," *IEEE Transactions on Microwave Theory and Techniques*, vol. 51, no. 3, 2003.

[31] Anritsu Measurement Guide, "Vector network analyzer for Anritsu RF and microwave handheld instruments," *Anritsu Company*, USA, 2016.

[32] C. A. Balanis, *Antenna Theory: Analysis and Design*. Wiley, New Jersey, USA, 2015.

[33] E. C. Fear, S. C. Hagness, P. M. Okoniewski, and M. Stuchly, "Enhancing breast tumor detection with near-field imaging," *IEEE Microwave Magazine*, vol. 3, no. 1, pp. 48-56, 2002.

[34] Y. Zhao, W. Shao, and G. Wang, "UWB microwave imaging for early breast cancer detection: Effect of two synthetic antenna array configurations," *IEEE International Conference on Systems, Man., & Cybernetics*, The Hague, Netherlands, 2004.

[35] M. Klemm, I. J. Craddock, J. A. Leendertz, A. Preece, and R. Benjamin, "Improved delay-and-sum beamforming algorithm for breast cancer detection," *International Journal of Antennas and Propagation*, pp. 1-9, 2008.

[36] G. Matrona, A. S. Savoia, G. Caliano, and G. Maganes, "The delay multiply and sum beam-forming algorithm in ultrasound B-mode medical imaging," *IEEE Transactions on Medical Imaging*, vol. 34, no. 4, pp. 940-949, 2014.

[37] S. I. Al-Mously and M. M. Abousetta, "A study of the hand on the EM interaction of a cellular handset and a human," *World Academy of Science, Engineering and Technology International Journal of Electronics and Communication Engineering*, vol. 2, no. 2, 2008.

[38] D. Yin, M. L. Li, and J. L. Li, "Non-invasive breast cancer thermotherapy studies using conformal microstrip antennas," in *Proc. ISAPE2012*, pp. 159-162, 2012.

[39] "International commission on non-Ionizing protection (ICNIRP) 1998 - Guidelines for limited exposure to time varying electric, magnetic and electromagnetic fields (up to 300 GHz)," *Health Physics*, vol. 74, no. 4, pp. 494-522, Apr. 1998.

[40] P. Bernardi, M. Cavagnaro, S. Pisa, and E. Piuzzi, "Specific absorption rate and temperature elevation in a subject exposed in the far-field of radio-frequency sources operating in the 10-900-mhz range," *IEEE Trans. Biomed. Eng.*, vol. 50, pp. 295-304, 2003.

[41] Y. Li, W. Li, and Q. Ye, "A reconfigurable triple notch band antenna integrated with defected

microstrip structure band-stop filter for ultra-wideband cognitive radio applications," *International Journal of Antennas and Propagation*, vol. 2013, Article ID:472645, pp. 1-13, 2013.

[42] Y. Li, W. Li, and W. Yu, "A switchable UWB slot antenna using SIS-HSIR and SIS-SIR for multi-mode wireless communications applications," *Applied Computational Electromagnetics Society (ACES) Journal*, vol. 27, no. 4, pp. 340-351, 2012.

[43] Y. Li, W. Li, and Q. Ye, "A compact circular slot UWB antenna with multimode reconfigurable band-notched characteristics using resonator and switch techniques," *Microwave and Optical Technology Letters*, vol. 56, no. 3, pp. 570-574, 2014.

[44] N. Ojaroudi, M. Ojaroudi, N. Ghadimi, and M. Mehranpour, "UWB square monopole antenna with omni-directional radiation patterns for use in circular cylindrical microwave imaging systems," *ACES Journal*, vol. 28, no. 2, pp. 123-129, 2013.

[45] M. Mokhtaari and J. Bornemann, "Directional ultrawideband antennas in planar technologies," in *Proc. 38th European Microwave Conference*, Amsterdam, Netherlands, 2008.

[46] A. Locatelli, D. Modotto, F. M. Pigozzo, S. Boscolo, E. Autizi, C. D. Angelis, A. D. Copabianco, and M. Midrio, "Highly directional planar ultrawide band antenna for radar applications," *European Microwave Conference*, Munich, Germany, 2007.

[47] F. Zhu, S. Gao, A. T. S. Ho, T. W. C. Brown, J. Z. Li and J. D. Xu, "Low-profile directional ultra-wideband antenna for see-through-wall imaging applications," *Progress In Electromagnetics Research*, vol. 121, pp. 121-139, 2011.

[48] J. J. Golezani, M. Abbak, and I. Akduman, "Modified directional wide band printed monopole antenna for use in radar and microwave ımaging applications," *Progress In Electromagnetics Research Letters*, vol. 33, pp. 119-129, 2012.

[49] I. Unal, B. Turetken, and C. Canbay, "Spherical conformal bowtie antenna for ultrawide band microwave imaging of breast cancer tumor," *Applied Computational Electromagnetics Society (ACES) Journal*, vol. 29, no. 2, pp. 124-133, 2014.

[50] M. L. Meena, M. Kumar, G. Parmar, and R. S. Meena, "Design analysis and modeling of directional UWB antenna with elliptical slotted ground structure for applications in C- & X-bands," *Progress In Electromagnetics Research-C*, vol. 63, pp. 193-207, 2016.

[51] A. M. Abbosh, "Directive antenna for ultra-wideband medical imaging systems," *International Journal of Antennas and Propagation*, pp. 1-6, 2008.

[52] A. R. Celik, "Simulation measurement for detection of the breast tumors by using ultra-wideband radar-based microwave technique," *International Research Journal of Engineering and Technology*, vol. 5, no. 11, pp. 1521-1525, 2008.

[53] X. Yun, E. C. Fear, and R. H. Johnston, "Compact antenna for radar-based breast cancer detection," *IEEE Transactions on Antennas and Propagation*, vol. 53, no. 8, pp. 2374-2380, 2005.

[54] W. C. Khor, M. E. Bialkowski, A. Abbosh, N. Seman, and S. Crozier, "An ultra wideband microwave imaging system for breast cancer detection," *IEICE Transactions on Communications*, vol. E90B, no. 9, pp. 2376-2381, 2007.

[55] M. Bialkowski and Y. Wang, "UWB cylindrical microwave imaging system employing virtual array antenna concept for background effect removal," *Microwave and Optical Technology Letters*, vol. 53, no. 5, pp. 1100-1104, 2011.

[56] S. Adnan, "Ultra-wideband antenna design for microwave imaging applications," *School of Eng., Design, and Tech. University of Bradford*, *PhD*, 2012.

[57] Y. Zhang, "Microwave imaging for ultra-wideband antenna based cancer detection," *The University of Edinburgh*, Scotland, *PhD*, 2014.

[58] I. Unal, "A new ultrawide-band (UWB) microwave imagıng system with minimized mutual coupling effects for breast tumor detection," *Yeditepe University*, Istanbul, Turkey, *PhD*, 2013.

[59] M. Abbak, "Antenna and measurement system for microwave imaging of breast tumors," *Istanbul Technical University*, *PhD*, 2015.

[60] M. A. Elahi, B. R. Lavoie, E. Porter, M. Glavin, E. Jones, E. C. Fear, and M. O'Halloran, "Comparison of radar-based microwave imaging algorithms applied to experimental breast phantoms," *32nd International Union of Radio Science General Assembly & Scientific Symposium*, Montreal, 2017.

Ali Recai Celik received his B.Sc. from the Gaziantep University, M.Sc. from the Sutcu Imam University and Ph.D. from the Dicle University, all in Rlectrical and Electronics Engineering. Since 2013, he has worked as a Research Assistant at Dicle University. His research interests are mainly antenna design and nondestructive testing of materials.

Muhammed Bahaddin Kurt received the B.Sc. and M.Sc. degrees from the Hacettepe University, Ankara in 1992 and 1996, respectively and Ph.D. degree from the Sakarya University, Turkey in 2002, all in Electrical and Electronics Engineering. He has been a member of Dicle University as an Assistant Professor since 2005 and as an Associate Professor since 2018. His research interests are mainly computational electromagnetics, microstrip patch antennas, and nondestructive testing of material.

Selcuk Helhel received his B.S. E.E. from Hacettepe University (1993), M.S. E.E. from Gebze Institute of Technology (1997) and Ph.D. E.E. from Sakarya University (2005). He has been a member of Akdeniz University as an Assistant Professor since 2006 and as a Full Professor since 2012. His research interests are microwave propagation, radar systems, EMC, EMI, WiMAX and WiMAX based video transmission, and capacity planning for telecommunication systems.